Journal of Materials Chemistry A

Accepted Manuscript

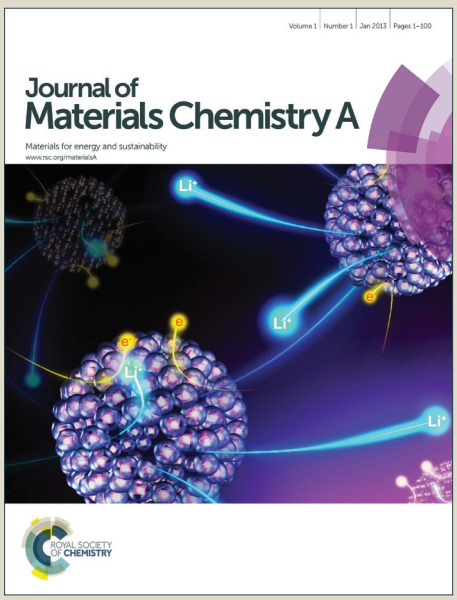

ROYAL SOCIETY OF CHEMISTRY

www.rsc.org/materialsA

Cite this: DOI: 10.1039/c0xx00000x

www.rsc.org/xxxxxx

ARTICLE TYPE

Rational design of diketopyrrolopyrrole-based oligomers for high performance small molecular photovoltaic materials *via* extended framework and multiple fluorine substitution

Qing-Ru Yin,[a][+] Jing-Sheng Miao,[b][+] Zhuo Wu,[a][+] Zheng-Feng Chang,[a] Jin-Liang Wang,*[a] Hong-Bin Wu,*[b] and Yong Cao[b]

Received (in XXX, XXX) Xth XXXXXXXXX 20XX, Accepted Xth XXXXXXXXX 20XX
DOI: 10.1039/b000000x

Two narrow-bandgap extended π-conjugated D_2-A_w-D_1-A_s-D_1-A_w-D_2 type small molecules (**DPPBIT** and **DPPBIT4F**) based on diketopyrrolopyrrole derivatives as the stronger acceptor core coupled with indacenodithiophene, benzothiadiazole or difluorobenzothiadiazole are designed and synthesized for application as donor materials in solution-processed small-molecule organic solar cells. The impacts of installation of four fluorine atoms to the two weaker acceptor units (benzothiadiazole) on the photophysical properties, the HOMO/LUMO energy level, charge carrier mobilities and the morphologies of blend films, and their photovoltaic properties are investigated. **DPPBIT** and **DPPBIT4F** possess similar broad and intense optical absorption covering the range from 300-900 nm and relatively low-lying HOMO energy levels. These two materials display significantly different photovoltaic performance. Compared with the best PCE of 2.7% for the blend films of **DPPBIT** and $PC_{71}BM$, the BHJ-OSC devices based on **DPPBIT4F** and $PC_{71}BM$, exhibited best PCE of 5.4% and very-high FF of 0.69 upon CH_2Cl_2 vapor annealing for 30 s, which is among one of the best reported photovoltaic performances based on DPP-core small molecules in single-junction BHJ solar cells. Exposure to CH_2Cl_2 vapor allows for a re-organization of the blend films, which increased the intensity and vibrational feature of absorption and dramatically improved the balance of charge carrier mobility and PCE.

Introduction

Solution-processed organic solar cells (OSCs) based on bulk-heterojunction (BHJ) device structures with narrow band gap π-conjugated molecules as donor and fullerene derivatives as acceptor have attracted considerable attention as a promising renewable energy resource because of their advantages such as light weight, flexibility, and low cost in recent years.[1] The development of donor/acceptor materials device architectures has led to record power conversion efficiencies (PCEs) of ca. 10% for soluble π-conjugated polymers in single-junction solar cells.[2] However, the polydispersity of polymers can represent these problems such as the reproducibility of the synthesis, purification, and electronic properties of the final active materials. Over the past few years, solution-processed narrow-bandgap small-molecules have gained increasing investigation because of their simple purification, monodisperse and well-defined structures, no end-group contaminants, and superior batch-to-batch reproducible performance compared to polymer counterparts.[3] Moreover, another advantage of small molecules is that they provide more reliable analyses of structure-properties-device performance relationships and disclose the key of the design of high performance photovoltaic materials. Therefore, the performance of solution processed BHJ-OSCs based on small-molecules has been dramatically increased over the past few years, which is approaching the best-performance of polymer solar cells.[4] Despite these best performance and high potential benefits, the typical building block for high performance (PCEs > 7%) small-molecule donor materials are still rather limited and countable, such as dithienosilole (DTS) core unit by Bazan and Heeger's groups, benzodithiophene (BDT) core units by Chen and Yang *et al.*, and porphyrin core units by Peng *et al.*[5] To enrich the pool of high performance small-molecule donor materials, the most straightforward and effective approaches are new molecular design, optimization on the films morphology and device engineering to in-depth understand the design principle of such donor materials.

To absorb the solar spectrum efficiently, these donor molecules are typical composed of multiple high optical density chromophores with push-pull characteristics. Diketopyrrolopyrrole (DPP), a typical strong acceptor chromophore with high molar extinction coefficient, has been investigated in small molecular organic solar cells.[6] Most of their HOMOs are relatively high, that always led to lower open circuit voltage (V_{oc}) of solar cells. By attaching of weaker aromatic donor units (phenyl, benzofuran, and pyrene) or electron-withdrawing unit (ester group), the HOMO of these materials has decreased, while the energy gap always becomes slight wider.[6]

Therefore, high-efficiency solar cells obtained from DPP-based small molecules were really rare and the best PCE of small molecular organic solar cells based on DPP derivatives was still below 6%,[6j,m] which is much lower than PCE obtained by DTS or BDT core. Another major drawback of DPP-based small molecules in blends with fullerene derivatives is the moderate fill factor (FF), caused by strong non-geminate recombination of DPP-based small molecules.[6] Thus, further improvement of the PCE requires that both the V_{oc} and the FF can be enlarged without deteriorating the favourable optical properties and high internal quantum efficiencies of DPP-based small molecules. Meanwhile, an popular strategy to improve the PCE by non-covalent ineraction is to attach fluorine atoms to the electron-deficient subnuits of conjugated polymer molecules.[7] Although the cause of the efficiency improvement varies noticeably depending upon the specific systems, it is generally accepted that monofluorinated or difluorinated benzothiadiazole as stronger acceptor chromophores can tune the optical and electronic properties of conjugated polymer materials, such as blue-shift of absorption peak and decrease of the HOMO energy level in comparison with their fluorine-free analogues.[8] Moreover, fluorine-sulfur or fluorine-hydrogen interactions often have great influence on inter-and intramolecular interaction, thus facilitate the formation of highly ordered solid-state structure and results in reducing charge recombination and higher device performance, relative to their fluorine-free analogues.[8] It remains a difficult task when incorporating multiple fluorine substituent (n>2) in a single small-molecule for highly efficient photovoltaic materials mainly due to less solubility of target materials. Moreover, less attention was paid on the impact of fluorine atoms on the weaker acceptor unit in extended backbone structures that having more than one acceptor units, particular for the influence on device performance with applying solvent annealing, thermal annealing or other post-treatments. These pioneering studies and challenge inspired us to synthesize new extended backbone structures with efficient light-harvesting and high carrier mobility by combining the existing merits of these two acceptor units (DPP as stronger acceptor and benzothiadiazole as weaker acceptor), which is essential to enhance the overall performance of solution-processed extended small-molecule solar cells based on DPP derivatives.

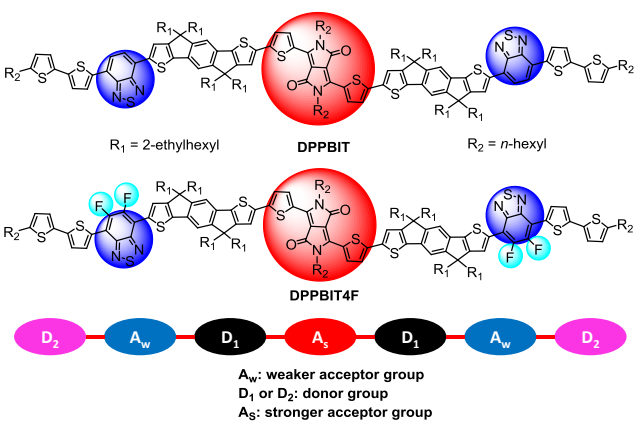

Chart 1. Structures of extended small molecular donor materials **DPPBIT** and **DPPBIT4F**.

Hence, we first describe the rational design and synthesis a series of extended π-conjugated small-molecules **DPPBIT** and **DPPBIT4F** based on the very similar extended molecular skeletons D_2-A_w-D_1-A_s-D_1-A_w-D_2. As shown in **Chart 1**, the two extended π-conjugated molecules both have a DPP-based core as the central stronger acceptor unit (A_s), two Indacenodithiophene (IDT)-based π-conjugated bridges as the donor (D_1), but with two benzothiadiazole or difluorobenzothiadiazole as the second and weaker acceptor (A_w), and two *n*-hexyl-substituted bithiophene as the terminal groups (D_2). Although the photophysical properties of these materials were dominated by the molecular backbone and stronger acceptor core, we are wondering that the impact of fluorine atoms on the weaker acceptor unit in extended backbone structures. Therefore, we focus our studies on evaluating the effect of installation two fluorine atoms on weaker acceptor (A_w)-benzothiadiazole or not on the bulk properties, such as the light-harvesting ability, the molecular HOMO/LUMO energy levels, charge carrier mobility, the morphologies of blend films, and photovoltaic performance parameters as donor material in the photoactive layer. These materials both exhibit good solubility in common organic solvents such as $CHCl_3$, THF, and toluene owing to the eight 2-ethylhexyls and four hexyls, thus they can be readily solution-processed and form excellent smooth films by spin-coating. In combination with using $PC_{71}BM$ as the acceptor, we discovered a striking difference of the photovoltaic behavior based on fluorinated materials and the fluorinated-free materials. The BHJ-OSC devices based on **DPPBIT4F**, that incorporating four fluorine atoms, exhibited PCE of 5.4%, with a high V_{oc} of 0.74 V, short circuit current density (J_{sc}) of 10.5 mA cm^{-2} and very-high FF of 0.69 for the device upon annealing by CH_2Cl_2 for 30 s without using any additives. There is 9 times increase of PCE in comparison with before solvent vapor annealing, which is particularly noteworthy that the initial performance as well as very-high FF is one of the best reported PCE based on DPP-core small molecules in single-junction BHJ solar cells. Surprisingly, the device based on non-fluorinated **DPPBIT** and $PC_{71}BM$ give much lower PCEs (2.7% of best results without solvent vapor annealing) and the PCE was reduced to 1.8% upon annealing by CH_2Cl_2 for 30 s, respectively. As mention in context, the prediction of bulk behavior of such materials as a function of chromophores connectivity remains in infant stage, thus it is still difficult to answer how to design a compound that would achieve high performance. The results herein provide a facile strategy to understand the impact of multiple fluorine atoms when attached to the weaker units of an extended conjugated D_2-A_w-D_1-A_s-D_1-A_w-D_2 framework. The reason that responsible to the impact is therefore of intense research interest and is investigated thoroughly in this study.

Results and discussion

Synthesis and thermal properties

The synthetic routes to these extended small molecules are shown in **Scheme 1**. Treatment of **1**[9] with *n*-BuLi followed by tributyltin chloride (1.0 eq.) facilely gave the monotin reagent **2** as light-yellow oil that was directly used in the next step without any further purification. **4** was prepared through the Stille coupling reactions between **2** and monobromide intermediate **3**[10] using a $Pd_2(dba)_3$/P(*o*-tolyl)$_3$ catalytic system. Then **4** can be

lithiated by LDA followed by quenching with trimethyltin chloride to afford monotin reagent **5**. Similarly, fluorinated intermediate **8** was obtained by a reaction sequence of Stille coupling reactions between another monobromide **6**[10] and monotin **2** and then treatment with LDA/Me_3SnCl in 46% overall yield. Finally, **DPPBIT** and **DPPBIT4F** were obtained through two-fold Stille coupling reaction between dibromide **9** and monotin **5**, **8** as dark solid in 76% and 81% isolated yield, respectively. All compounds were purified by silica gel column chromatography, and their structures and purity were verified by ^1H and ^{13}C NMR, elemental analysis, and ESI/MALDI-TOF MS. The thermal property of these extended small molecules was investigated by thermogravimetric analysis (TGA) **(Figure S1)**. Under N_2 atmosphere, the onset temperature with 5% weight-loss is about 408 °C for **DPPBIT** and 410 °C for **DPPBIT4F,** respectively, which indicated that the thermal stability of these molecules is adequate for application in organic solar cells.

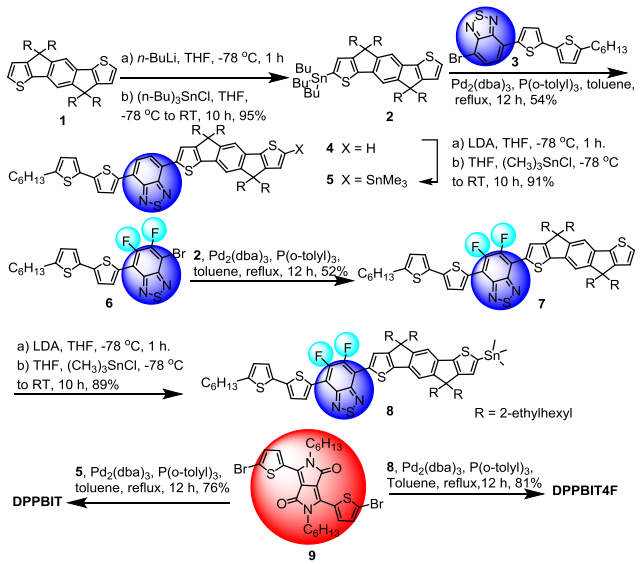

Scheme 1. Synthesis of extended small molecules **DPPBIT** and **DPPBIT4F**.

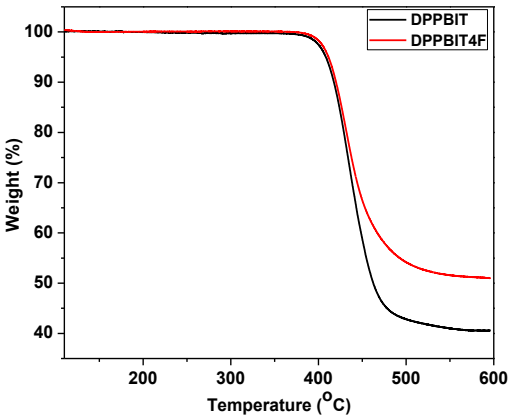

Figure 1. TGA of **DPPBIT** and **DPPBIT4F** with a heating rate of 10 °C/min under N_2 atmosphere.

Optical properties

To investigate the relationship between the molecular structure and the photophysical property, the absorption spectra of these extended small-molecules both in diluted chloroform solutions and in thin films obtained by spin-coating were recorded in **Figure 2**. Two molecules showed two distinct absorption bands (Band I: 350-450 nm; Band II: 450-900 nm) in solution and solid state due to π-π* transition of conjugated backbone and the intramolecular charge transfer (ICT) between two molecular donor and two acceptor units. Two compounds have structured vibrational absorption peaks in the Band II region, which agrees well with their shaped-persistent conjugated backbones. Very interesting, although the spectral profile of **DPPBIT4F** is nearly identical to that of the nonfluorinated **DPPBIT** in solution, introduction of four fluorine atoms in **DPPBIT4F** exhibited a slight blue-shift by ca. 2 nm, 5 nm, and 3 nm at three λ_{max} peaks (0-0 and 0-1 vibrational peaks in Band II region and λ_{max} peak in Band I region) in comparison with these of **DPPBIT**, respectively. In addition, two compounds show different oscillator strength of vibrational absorption peaks in Band II region. For example, compared with **DPPBIT**, the obvious shoulder features at about range of 500-600 nm with higher molar extinction coefficient are shown in the spectra of **DPPBIT4F**, which might be attributed to the increase in molecular rigidity and planarity through the fluorine-sulfur or fluorine-hydrogen interactions between benzothiadiazole and IDT units.[11] In contrast, the absorption spectra of these extended small molecules in thin films are obviously red-shifted and increased the relative intensity of their 0-0 vibrational peak. Compared to those main absorption maximum peaks (λ_{max}) at about 700 nm in solutions, **DPPBIT** and **DPPBIT4F** both display red-shift of ca. 26 nm in the thin films. Moreover, **DPPBIT4F** still exhibited a slight blue-shift (ca. 3 nm) of λ_{max} peak at about 700 nm in comparison with these of **DPPBIT** in the thin film. Such features are attributed to a more planar conjugated backbone and more ordered structure in the solid state. Therefore a higher π-electron delocalization through the whole molecular backbone and enhanced interchromophore interactions is expected, which could be beneficial to a higher hole mobility. From the onset of absorption in thin films, the optical band gap of solid states were estimated to be 1.60 eV for **DPPBIT** and 1.61 eV for **DPPBIT4F**, respectively, as listed in **Table 1**. This indicates that the introduction of four fluorine atoms on weaker acceptor unit (benzothiadiazole) in DPP-based extended linear small molecules does not obviously affect the band gap.

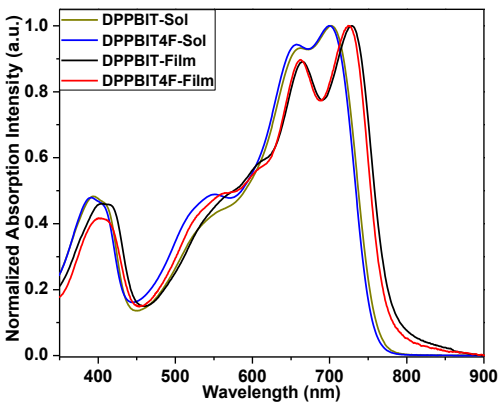

Figure 2. The absorption spectra of **DPPBIT** and **DPPBIT4F** in chloroform solutions (2×10^{-6} M) and in the thin films measured at room temperature.

Table 1. Photophysical properties of **DPPBIT** and **DPPBIT4F** in

solutions and in the thin films.

Compd	λ_{max}abs. (sol) (nm)	λ_{max}abs. (film) (nm)	$E_{g(opt)}$[a] (eV)
DPPBIT	703, 662, 393	729, 665, 404	1.60
DPPBIT4F	700, 657, 551, 391	726, 662, 404	1.61

[a]estimated from the onset of thin-film absorption.

Electrochemical properties

In order to investigate the relationship between the chemical structures and the electrochemical properties of the desired materials, the cyclic voltammetry (CV) experiments of two materials in thin films were conducted. The CV curves showed one quasi-reversible *p*-doping process and *n*-doping process (**Figure 3**). After introducing fluorine atoms, the reductive doping processes of **DPPBIT4F** appear to be slight more reversible than those of **DPPBIT**. The HOMO and LUMO levels are -5.22 eV/-3.26 eV for **DPPBIT** and -5.23 eV/-3.27 eV for **DPPBIT4F**, respectively, according to the following equation of E_{HOMO} = -e(E_{Ox}+4.80) (eV) and E_{LUMO} = -e(E_{red}+4.80) (eV). **DPPBIT4F** showed slight deeper HOMO levels (ΔE = 0.03 eV) relative to **DPPBIT** due to the electronic withdrawing nature of four fluorine groups on the two weaker acceptor units (benzothiadiazole). In contrast, changes in LUMO energy levels on fluorine substitution are less notable because the LUMOs are mostly localized on the stronger electron-deficient cores (DPP) of the extended compounds, which result in a slight increase of the band gap of **DPPIDTBF.** The electrochemical band gaps ($E_{g(cv)}$) albeit slightly larger than the corresponding optical band gaps ($E_{g(opt)}$) because states measured in the electrochemical experiments (free ions) and that of the optical results (neutral states) are somewhat different. Such slight decrease of HOMO energy level for **DPPBIT4F** may be good for its BHJ-OSCs performances.

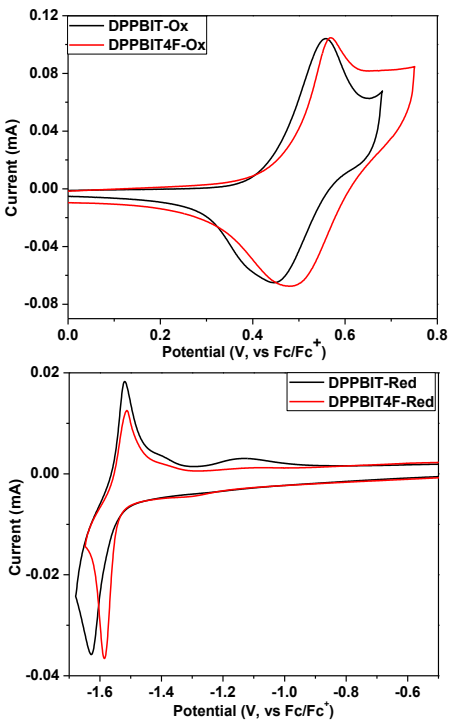

Figure 3. Cyclic voltammogram of **DPPBIT** and **DPPBIT4F** films on Pt electrode in 0.1 M Bu_4NPF_6 in CH_3CN solution with a scan rate of 50 mV/s.

Table 2. Electrochemical properties of **DPPBIT** and **DPPBIT4F** in the thin films on Pt electrode.

Compd	$E_{ox(onset)}$[a] (V)	$E_{red(onset)}$[a] (V)	E_{HOMO} (eV)	E_{LUMO} (eV)	$E_{g(cv)}$ (eV)
DPPBIT	0.40	-1.54	-5.20	-3.26	1.94
DPPBIT4F	0.43	-1.53	-5.23	-3.27	1.96

[a]potentials are measured relative to a Fc/Fc^+ redox couple as an external reference (-4.8 eV in vacuum).

Photovoltaic properties

Table 3. A summary of the device performances of the organic solar cells from blend films of the **DPPBIT** and **DPPBIT4F** as donor materials and **$PC_{71}BM$** as the acceptor.

Active layer	Jsc (mA/cm^2)	V_{oc} (V)	FF (%)	PCE (%)
DPPBIT/$PC_{71}BM$ (1:3)	8.4	0.80	40	2.7
DPPBIT/$PC_{71}BM$ (1:3)[a]	4.8	0.77	48	1.8
DPPBIT/$PC_{71}BM$ (1:3)[b]	8.8	0.80	39	2.7
DPPBIT/$PC_{71}BM$ (1:3)[c]	7.8	0.77	45	2.7
DPPBIT/$PC_{71}BM$ (1:3)[d]	6.2	0.80	46	2.3
DPPBIT/$PC_{71}BM$ (1:2)	7.9	0.82	38	2.4
DPPBIT/$PC_{71}BM$ (1:2)[a]	5.0	0.78	43	1.7
DPPBIT/$PC_{71}BM$(1:1)	2.7	0.83	29	0.7
DPPBIT/$PC_{71}BM$(1:1)[a]	2.7	0.78	44	0.9
DPPBIT/$PC_{71}BM$ (1:0.8)	1.9	0.83	27	0.4
DPPBIT/$PC_{71}BM$ (1:0.8)[a]	1.8	0.79	34	0.5
DPPBIT4F/$PC_{71}BM$ (1:3)	6.6	0.81	37	2.0
DPPBIT4F/$PC_{71}BM$ (1:3)[a]	7.4	0.75	65	3.6
DPPBIT4F/$PC_{71}BM$ (1:2)	5.2	0.83	34	1.5
DPPBIT4F/$PC_{71}BM$ (1:2)[a]	9.8	0.73	66	4.7
DPPBIT4F/$PC_{71}BM$ (1:1.5)	3.9	0.85	33	1.1
DPPBIT4F/$PC_{71}BM$ (1:1.5)[a]	8.9	0.74	71	4.6
DPPBIT4F/$PC_{71}BM$ (1:1)	2.5	0.84	29	0.6
DPPBIT4F/$PC_{71}BM$(1:1)[a]	10.5	0.74	69	5.4
DPPBIT4F/$PC_{71}BM$(1:1)[b]	2.5	0.85	29	0.6
DPPBIT4F/$PC_{71}BM$(1:1)[c]	11.0	0.73	66	5.3
DPPBIT4F/$PC_{71}BM$(1:1)[d]	3.9	0.57	14	0.3
DPPBIT4F/$PC_{71}BM$ (1:0.8)	1.5	0.83	27	0.3
DPPBIT4F/$PC_{71}BM$ (1:0.8)[a]	8.5	0.74	62	3.9
DPPBIT4F/$PC_{71}BM$ (1:0.6)	0.9	0.84	26	0.2
DPPBIT4F/$PC_{71}BM$ (1:0.6)[a]	7.5	7.5	60	3.3

[a] treatment with CH_2Cl_2 vapor for 30 s; [b] thermal annealing at 80 °C for 10 min; [c] thermal annealing at 80 °C for 10 min and then treatment with CH_2Cl_2 vapor for 30 s; [d]0.4% DIO was added into solvent.

To demonstrate the potential of these extended small-molecules **DPPBIT** and **DPPBIT4F** as promising donor materials in organic solar cells, we fabricated BHJ-OSCs with a device structure ITO/PEDOT:PSS/small molecule donor: $PC_{71}BM$)/PFN/Al. The blend ratio significantly influenced the

device performance. As an effective method for enhancement of PCE, solvent vapor annealing has been used in BHJ-OSCs to optimize the morphology of the active layer.[12] Herein, the method was used in the device optimization in combination with different D/A ratio (1:3, 1:2, 1:1.5, 1:1, 1:0.8, 1:0.6 for **DPPBIT4F,** and 1:3, 1:2, 1:1, 1:0.8 for **DPPBIT**). For solvent vapor annealing, the active layer was exposed to CH_2Cl_2 for 30 s, without the need of incorporation of additive. The optimized thicknesses of the active layers were determined to be 80-100 nm. **Table 3** summarizes the device performance for two materials before and after solvent vapor annealing, such as V_{oc}, J_{sc}, FF, and PCE of the devices under 1 sun illumination. As expected, all of the devices based on our two small-molecules exhibited high V_{oc} (0.74-0.85 V) due to the relative lower-lying HOMO energy levels of donor materials, although V_{oc} slightly decreased after solvent vapor annealing under the same D/A ratio.[13] It is worthy to mention, the reduction in V_{oc} after solvent vapor annealing is very common in solution-processed small-molecule organic solar cells,[12] which will be discussed later.

Before the solvent vapor annealing method is applying the two materials, the best PCE is 2.7% for **DPPBIT** and 2.0% for **DPPBIT4F** with $PC_{71}BM$ by 1:3 ratios. It is indicated that the devices performance is not big different from the two materials. After the solvent vapor annealing method is applying, for **DPPBIT**/$PC_{71}BM$ (1:3 and 1:2) based devices, the photovoltaic performance was reduced to 1.8% and 1.7% upon annealing by CH_2Cl_2 for 30 s, respectively. Moreover, **DPPBIT** with 1:1 ratio of $PC_{71}BM$ slightly improved in efficiency after solvent vapor annealing with CH_2Cl_2. Surprising, **DPPBIT4F** blends with $PC_{71}BM$ dramatically improved the PCE due to significant enhancement of J_{sc} and FF as a result of exposure to CH_2Cl_2 vapor. For example, the optimal performance was obtained when the weight ratio of **DPPBIT4F**/$PC_{71}BM$ is 1:1, which resulted in a J_{sc} = 10.5 mA cm^{-2}, V_{oc} = 0.74 V, FF = 0.69, and PCE =5.4%.

In order to further improve the photovoltaic performance of **DPPBIT4F** when the weight ratio of **DPPBIT4F**/$PC_{71}BM$ is 1:1, the thermal annealing at 80 °C for 10 min and addition of additive diiodooctane (DIO) was employed in the device optimization in combination with solvent vapor annealing. Surprising, after **DPPBIT4F** was solely treated by thermal annealing at 80 °C for 10 min, the PCE kept at about 0.6%. When the thermal annealing active layer was exposed CH_2Cl_2 vapor for 30 s, the PCE also sharply improved to 5.3%, with a J_{sc} = 11.0 mA cm^{-2}, V_{oc} = 0.73 V, and FF = 0.66. However, when 0.4% DIO was added into solvent, the PCE dramatically decreased to 0.3%. It seems that solvent vapor annealing is more efficient method for our materials to improve the PCE than the thermal annealing and addition of additive. Using of solvent vapor annealing can caused about 9 times increase of PCE, over 4 times increase of J_{sc}, over 2 times increase of FF, and slight drop of V_{oc} in comparison with without solvent vapor annealing, which is particularly noteworthy that the initial performance as well as very-high FF is one of the best reported PCE based on DPP-core small molecules in the literature.

Considering the fact that **DPPBIT** and **DPPBIT4F** are similar with a structural variation only with or without the four fluorine groups, the effect of introduction of F atoms on the large difference of photovoltaic performance is amazing. The high PCE of **DPPBIT4F** based OSCs by post-treatment further proved that the introduction of fluorine atom to molecules is a valid design strategy for high performance OSCs. Moreover, as shown in table 3, the device performance of **DPPBIT** is better than that of **DPPBIT4F** under thermal annealing and addition of additive or without the solvent vapor annealing for the two materials. However, after solvent vapor annealing, the device performance of **DPPBIT4F** is much better than that of **DPPBIT.** The higher ratios of **DPPBIT4F** in the blends with $PC_{71}BM$ (from 1:3 to 1:0.6), the bigger difference of performance (1.8 times to 16.5 times) was observed for **DPPBIT4F** with or without solvent vapor annealing. It seems that solvent vapor annealing play critical positive roles on **DPPBIT4F** with the multiple fluorine substitution in OPV application in comparison with **DPPBIT,** which is probably facilitate the formation of highly ordered solid-state structure and get higher device performance after solvent vapor annealing as discussed below.[12]

Figure 4 showed the current density versus voltage (*J-V*) characteristics of the best device from **DPPBIT4F: $PC_{71}BM$** (1:1) and **DPPBIT: $PC_{71}BM$** (1:3) before and after solvent vapor annealing. For comparison, the best *J-V* characteristics of other device from other ratios are also shown (see **Figure S1**). The substantial J_{sc} improvement (7.4 mA cm^{-2} vs. 10.5 mA cm^{-2}) upon the change of blend ratio of **DPPBIT4F** and PCBM from 1:3 to 1:1 both treated with solvent vapor annealing can be partially attributed to stronger optical absorption coverage in whole visible region, which can be clearly seen from **Figure 5**. Indeed, the blend film with 1: 1 ratio of **DPPBIT4F**/$PC_{71}BM$ showed an obvious enhancement in absorption spectra in the range of 450-800 nm when compared with the film from the 1: 3 blends.

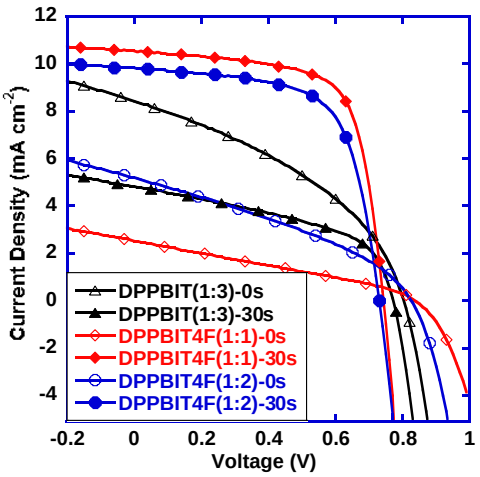

Figure 4: Current density-voltage (*J-V*) characteristics of the best OSC devices based on **DPPBIT** and **DPPBIT4F** blend with **$PC_{71}BM$** (different blend ratio and before/after CH_2Cl_2 vapor annealing).

To determine the origin of the observed photovoltaic performance differences between **DPPBIT** and **DPPBIT4F** as well as the effect of solvent vapor annealing on the active layer, we carried out more detailed investigations on absorption properties, external quantum efficiency (EQE), their charge mobility, and morphology of blend films by atomic force microscopy (AFM) to draw structure-property relationship.

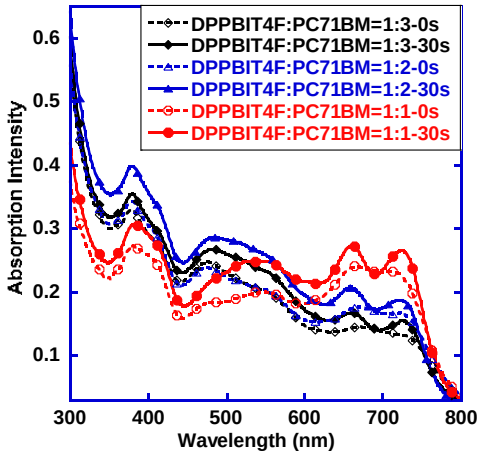

Figure 5: Absorption spectra of **DPPBIT4F:** $PC_{71}BM$ (1:1, 1:2, and 1:3, w/w) blend films with or without CH_2Cl_2 vapor annealing.

As shown in **Figure 5**, in comparison with the absorption spectra of as-cast the blend film of **DPPBIT4F** with **$PC_{71}BM$** (1:1 to 1:3), the spectra of the film with CH_2Cl_2 vapor annealing showed well-defined features across the entire visible spectrum. For example, there is much obvious 0-0 and 0-1 vibrational shoulder peaks and the absorption intensity at range of 450-800 nm overall obviously increased, particular for 1:1 and 1:2 ratio, which is related to the enhanced π-π stacking and interaction of intermolecules by the increase in molecular planarity between difluorinated benzothiadiazole and IDT units. Such enhanced absorption features results in improved J_{sc} from 2.5 mA cm^{-2} to 10.5 mA cm^{-2} for blend films by 1:1 ratio of **DPPBIT4F:** $PC_{71}BM$ after CH_2Cl_2 vapor annealing. In contrast, as shown in **Figure S3**, in comparison with the absorption spectra of as-cast the blend film of **DPPBIT** with **$PC_{71}BM$** (1:1 to 1:3) , the spectra of the film on CH_2Cl_2 vapor annealing exhibited only slight increase of absorption intensity, but had very similar absorption profile.

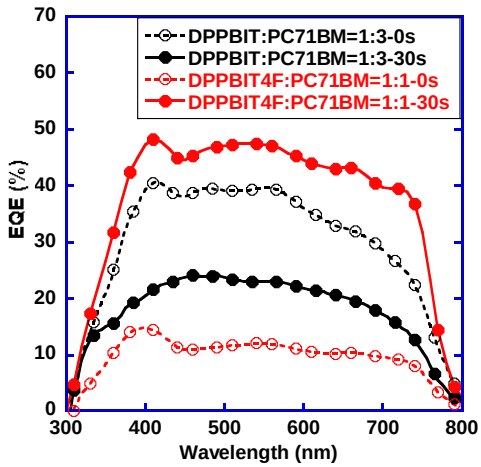

Figure 6. EQE plots of the best OSC devices based on **DPPBIT** or **DPPBIT4F** blend with **$PC_{71}BM$** before/after CH_2Cl_2 vapor annealing.

To further understand the device performance, the external quantum efficiencies (EQE) spectra of these devices were measured and shown in **Figure 6**. All the EQE spectra covered a broad wavelength range from 300-800 nm for all the devices based on **DPPBIT** and **DPPBIT4F**. It is apparent that exposure to CH_2Cl_2 vapor leads to increased EQE in the entire photoactive region for **DPPBIT4F**-based devices, which is consistent with the increase in J_{sc}. For example, the maximum EQE value is 15% at 400 nm and 48% at 410 nm for these devices based on **DPPBIT4F:$PC_{71}BM$** (1:1) blend without and with solvent vapor annealing treatment, respectively, which indicates that the photoelectron conversion process is more efficient after solvent vapor annealing. Moreover, the blend film with 1: 1 ratio of **DPPBIT4F**/$PC_{71}BM$ showed an obvious enhancement in the EQE profile, particular for the range of 600-800 nm when compared with the film from the 1: 3 blend both after solvent treatment (see Figure S4). These results are consistent with the trend of the above Uv-vis absorption results. However, although the shape and intensity of absorption spectra remained unaffected by the CH_2Cl_2 vapor annealing for blend films with **DPPBIT**/$PC_{71}BM$, the intensity of EQE spectra was obviously decreased in the entire photoactive region for the blend film with 1: 3 ratio of **DPPBIT**/$PC_{71}BM$ under CH_2Cl_2 vapor annealing. The calculated J_{sc} values obtained by integration of the EQE data for these devices showed 2-5% mismatch compared with the J_{sc} value from *J*-V curve.

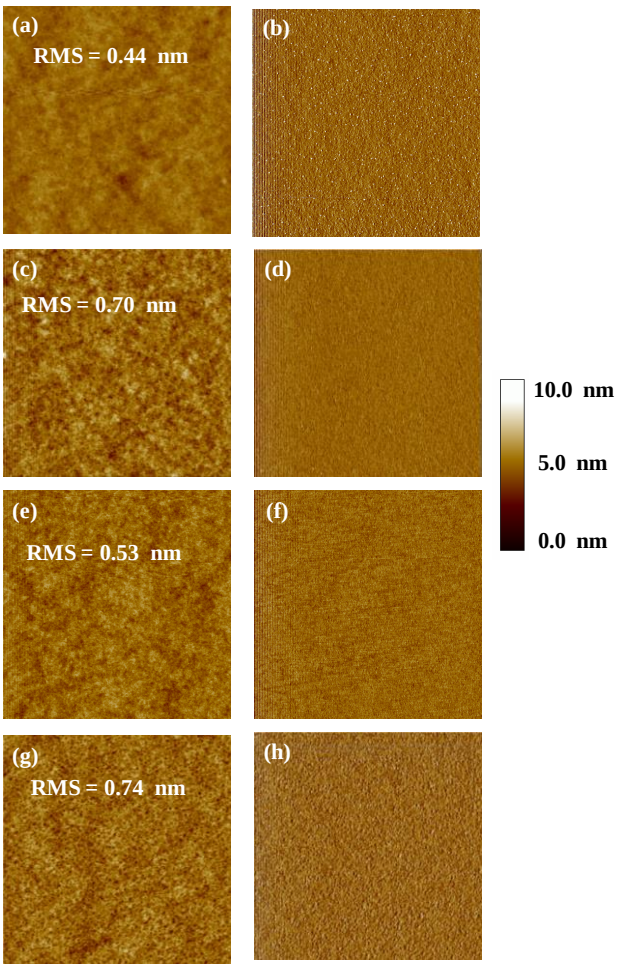

Figure 7. Tapping mode AFM height (a, c, e, g) and phase (b, d, f, h) images 5×5 μm^2 of (a, b) **DPPBIT4F/PC$_{71}$BM** (1:1, w/w); (c, d) **DPPBIT4F/PC$_{71}$BM** (1:1, w/w) after CH_2Cl_2 vapor annealing; (e, f) **DPPBIT/PC$_{71}$BM** (1:3, w/w); (g, h) **DPPBIT/PC$_{71}$BM** (1:3, w/w) after CH_2Cl_2 vapor annealing.

It is well known that film morphology plays a key role in the charge separation and charge transfer for the organic thin film solar cells. To investigate the causes for the enhanced OSC performances of **DPPBIT4F**, the film morphologies were measured using tapping mode AFM. The samples were prepared by spin-coating the donor: PC$_{71}$BM blend in the same way as the photoactive layers for the solar cell devices. Without solvent annealing, large parts of the film surface were smooth and featureless with a root-mean-square roughness (R_{rms}) of about 0.4-0.5 nm, indicating all of the donor materials have a good miscibility with PC$_{71}$BM. After solvent vapor annealing, the blend films were more phase-separated, displayed larger surface aggregates. The roughness of the film surface increased after solvent vapor annealing from 0.44 nm to 0.70 nm for the blend of 1: 1 ratio of **DPPBIT4F**/PC$_{71}$BM and from 0.53 nm to 0.74 nm for the blend of 1: 3 ratio of **DPPBIT**/PC$_{71}$BM, respectively, as a result of the enhanced intermolecular interactions among the small molecular donor in the active layer, as indicated by the optical properties of the blend films, which was in good agreement with a previous literatures.[14] Obviously, the solvent vapor annealing provided a driving force to increase in the domain and the more ordered film morphology of the active layer in nanoscale, which is preferable to improve charge transport properties upon solvent treatment as discussed below.

Table 4. A summary of the charge carrier mobilities from blend films of the **DPPBIT** or **DPPBIT4F** and **PC$_{71}$BM** before/after CH_2Cl_2 vapor annealing.

Active layer	μ_e ($cm^2 V^{-1} s^{-1}$)	μ_h ($cm^2 V^{-1} s^{-1}$)	μ_e/μ_h ratio
DPPBIT/PC$_{71}$BM(1:3)	3.1×10^{-4}	1.0×10^{-5}	31
DPPBIT/PC$_{71}$BM(1:3)[a]	1.5×10^{-4}	3.3×10^{-5}	4.5
DPPBIT/PC$_{71}$BM(1:2)	2.2×10^{-4}	2.1×10^{-5}	10.5
DPPBIT/PC$_{71}$BM(1:2)[a]	1.7×10^{-4}	3.5×10^{-5}	4.9
DPPBIT4F/PC$_{71}$BM(1:2)	2.4×10^{-4}	1.3×10^{-5}	18.5
DPPBIT4F/PC$_{71}$BM(1:2)[a]	1.5×10^{-4}	2.5×10^{-4}	0.6
DPPBIT4F/PC$_{71}$BM(1:1)	9.6×10^{-5}	2.3×10^{-5}	4.2
DPPBIT4F/PC$_{71}$BM(1:1)[a]	6.8×10^{-5}	9.7×10^{-5}	0.7

[a] treatment with CH_2Cl_2 vapor for 30 s

To verify the positive effect of the solvent vapor annealing on charge transporting and understand the relationship between the charge carrier transport properties and structure of these two extended small molecules blend with PC$_{71}$BM, the charge carrier mobilities were determined from space charge limited current (SCLC) measurements in the actual device before and after solvent vapor annealing procedure. The structures of hole only and electron only device are ITO/PEDOT/donor materials: PC$_{71}$BM/MoO_3/Al and ITO/ZnO/PFN/ donor materials: PC$_{71}$BM/Ca/Al, respectively. **Table 4** displays the hole and electron mobilities determined from the SCLC measurements and **Figure S5** displays *J-V* characteristics of the hole-only or electron-only devices as obtained in dark. The hole mobility for device fabricated from **DPPBIT** or **DPPBIT4F** was enhanced after CH_2Cl_2 vapor annealing for 30 s, which is consistent with increase of R_{rms} in AFM image. For example, for devices without CH_2Cl_2 vapor annealing based on 1: 1 ratio of **DPPBIT4F**/PC$_{71}$BM and 1: 3 ratio of **DPPBIT**/PC$_{71}$BM, the hole mobility were 2.3×10^{-5} $cm^2 V^{-1} s^{-1}$ and 1.0×10^{-5} $cm^2 V^{-1} s^{-1}$, respectively. After CH_2Cl_2 vapor annealing for 30 s, the hole mobility increased to 9.7×10^{-5} $cm^2 V^{-1} s^{-1}$ and 3.3×10^{-5} $cm^2 V^{-1} s^{-1}$, respectively, which is correspond to a higher than three times enhancement. Although the electron mobility for most original device is higher than corresponding hole mobility, the electron mobility was slightly decreased after CH_2Cl_2 vapor annealing for 30 s. As mentioned above, the μ_e/μ_h ratio is 0.7 for device based on 1: 1 ratio of **DPPBIT4F**/PC$_{71}$BM and 4.5 for device based on 1: 3 ratio of **DPPBIT**/PC$_{71}$BM after CH_2Cl_2 vapor annealing for 30 s, which dramatically decreased in comparison with the corresponding μ_e/μ_h ratio before the solvent treatment (4.2 for **DPPBIT4F** and 31 for **DPPBIT**). These results (higher and much balanced carrier mobility) suggest that CH_2Cl_2 vapor annealing is beneficial to the higher FF compared to original devices. Indeed, after solvent vapor annealing, device based on **DPPBIT4F** or **DPPBIT**/PC$_{71}$BM can obtain improved FF, particular for **DPPBIT4F** with very high FF (up to 71%) due to the much more balanced hole and electron mobility in comparison with device based on **DPPBIT**/PC$_{71}$BM. The more balanced and higher mobility contributes to higher J_{sc} and FF because the accumulated charges and recombination processes are reduced by the increase in the carrier mobility and enhanced charge collection efficiency.[15] On the other side, the more balanced hole and electron mobility and favourable charge extraction can lead to a depleted steady carrier density in the active layer, [12b, 13b, 16] thus will result in a concomitant lower quasi-Fermi levels for electron and hole transport and reduction in V_{oc}.

Conclusions

In this study, two DPP core-based extended conjugated D_2-A_w-D_1-A_s-D_1-A_w-D_2 type small molecules, **DPPBIT** or **DPPBIT4F** have been designed and synthesized as donor for BHJ-OSCs. The installation of four fluorine atoms to the two weaker acceptor (benzothiadiazole) of **DPPBIT4F** do not show obvious influence on the optical and electrochemical properties of **DPPBIT4F** compared with these of fluorine-free **DPPBIT**. However, compared with the best PCE of 2.7% for **DPPBIT** and PC$_{71}$BM, the BHJ-OSC devices based on **DPPBIT4F** and PC$_{71}$BM, exhibited best PCE of 5.4% and very-high FF of 0.69 for the device upon annealing by CH_2Cl_2 for 30 s but without using any additives, which is among one of the best reported photovoltaic performances based on DPP-core small molecules in single-junction BHJ solar cells, particular for very-high FF (up to 71% for some devices). These amazing results have revealed how large impacts on the photovoltaic performances can be achieved by installation of four fluorine atoms or not to weaker acceptor units as well as solvent vapor annealing. Exposure to CH_2Cl_2 vapor allows for a re-organization of the blend, which increased

the intensity and vibrational feature of absorption, improved the balance of charge carrier mobility and PCE. Throughout this study, one may understand the importance of attachment of fluorine atoms on the weaker acceptor units in extended conjugated structure to materials photovoltaic performance. Moreover, the larger performance difference between these two compounds proves a valid design strategy for high performance optoelectronic materials.

Experimental Section

Materials and Chracterization: All air and water sensitive reactions were performed under nitrogen atmosphere. Tetrahydrofuran (THF) was dried over Na/benzophenone ketyl and freshly distilled prior to use. The other materials were of the common commercial level and used as received. Thin layer chromatography (TLC) was conducted on flexible sheets precoated with SiO_2 and the separated products were visualized by UV light. Column chromatography was conducted using SiO_2 (300 mesh) from Fisher Scientific. ^1H and ^{13}C NMR spectra were recorded on a Bruker ARX-400 (400 MHz) or ARX-500 (500 MHz) spectrometer, using $CDCl_3$, except where noted. All chemical shifts were reported in parts per million (ppm). ^1H NMR chemical shifts were referenced to TMS (0 ppm), and ^{13}C NMR chemical shifts were referenced to $CDCl_3$ (77.23 ppm). MALDI-TOF-MS was recorded on a Bruker BIFLEX III mass spectrometer. Thermal gravity analyses (TGA) were carried out on a TA Instrument Q600 analyzer. Elemental analyses were performed using a German Vario EL III elemental analyzer. Absorption spectra were recorded on PerkinElmer Lambda 750 UV-vis spectrometer. Cyclic voltammetry (CV) was performed on BASI Epsilon workstation. Glassy carbon electrode was used as a working electrode and a platinum wire as a counter electrode. These films were drop-cast on a glass carbon working electrode from THF at a concentration of 5 mg/mL. Measurements were carried out at a scan rate of 50 mV/s in CH_3CN containing 0.1 M n-Bu_4NPF_6 as the supporting electrolyte. All potentials were recorded versus Ag/AgCl reference electrode and calibrated with the redox couple of Fc/Fc^+ under the same experimental conditions.

BHJ-OSC fabrication, characterization and measurement: Device preparation and characterization were carried out in clean room conditions with protection against dust and moisture. The fabrication of BHJ-OSCs followed the procedures described in our previous paper.[17] The values of power conversion efficiency were determined from *J*-V characteristics measured by a Keithley 2400 source-measurement unit under AM 1.5G spectrum from a solar simulator (Oriel model 91192). Masks made from laser beam cutting technology with well-defined area of 16.0 mm^2 were attached to define the effective area for accurate measurement. Solar simulator illumination intensity was determined using a monocrystal silicon reference cell (Hamamatsu S1133, with KG-5 visible color filter) calibrated by the National Renewable Energy Laboratory (NREL). The active layer was spin-coated from blend chloroform solutions with weight ratio of **DPPBIT** or **DPPBIT4F** and $PC_{71}BM$ at 1:1 (or other ratios) and then were placed in a glass petri dish containing 1 mL CH_2Cl_2 for 30 s for solvent vapor annealing. The film morphology was studied by atomic force microscopy (AFM, Veeco MultiMode V) operating in tapping mode. EQE values of the encapsulated devices were measured by using an integrated system (Enlitech, Taiwan, China) and a lock-in amplifier with a current preamplifier under short-circuit conditions. The devices were illuminated by monochromatic light from a 75 W xenon lamp. The light intensity was determined by using a calibrated silicon photodiode.

Synthesis:

2: To a solution of **1** (1.06 g, 1.49 mmol) in anhydrous THF was added dropwise a hexane solution of *n*-butyllithium (0.65 mL, 1.50 mmol) in N_2 atmosphere at -78 ℃. The reaction mixture was stirred at this temperature for 1 h. Tributhyltin chloride (0.41 mL, 1.50 mmol) was added dropwise into the mixture at -78 ℃. The reaction mixture was allowed to warm to room temperature and stirred for 10 h. The mixture solution was quenched with water, and extracted with chloroform. The organic extracts were washed with brine and dried over anhydrous Na_2SO_4. After removal of the solvent under the reduced pressure, the monotin compound as the mainly product was obtained as light yellow oil (1.75 g, 95%) and used in the next step without any further purification.

4: In a 100 mL two-neck round-bottom flask, **2** (250 mg, ca. 0.25 mmol), **3** (116 mg, 0.25 mmol), and $Pd_2(dba)_3$ (11.5 mg, 0.013 mmol), tri(*o*-tolyl) phosphine (15.5 mg, 0.051 mmol) was added. The flask was evacuated and back-filled with N_2 three times, and then degassed toluene was injected into the mixture. The resulting solution was stirred at refluxing temperature for 12 h under the N_2 atmosphere. After being cooled to room temperature, the solvent was then removed under reduced pressure. The dark residue was purified by silica gel chromatography, eluting with petroleum ether (PE)-CH_2Cl_2 (20:1) to give purple solid (148 mg, 54%). ^1H NMR ($CDCl_3$, 400 MHz, ppm): δ 8.08-8.16 (m, 1H, Th-H), 8.02-8.04 (m, 1H, Th-H), 7.83-7.89 (d, d, *J* = 7.6 Hz, 2H, Ph-H), 7.40 (s, 1H, Ph-H), 7.35 (s, 1H, Ph-H), 7.24-7.25 (d, *J* = 4.8 Hz, 1H, Th-H),7.20-7.21 (d, *J* = 3.6 Hz, 1H, Th-H), 7.11-7.12 (d, *J* = 3.6 Hz, 1H, Th-H), 6.98-6.99 (m, 1H, Th-H), 6.73-6.74 (d, *J* = 3.6 Hz, 1H, Th-H), 2.81-2.85 (t, *J* = 7.6 Hz, 2H, CH_2), 1.98-2.05 (m, 8H, CH_2), 1.68-1.75 (m, 2H, CH_2), 1.32-1.43 (m, 6H, CH_2), 0.53-0.97 (m, 63H, CH_2, CH_3). ^{13}C NMR ($CDCl_3$, 100 MHz, ppm): δ (155.80, 155.76), (155.3, 155.2, 155.1), 153.4, 153.2, 152.8, 152.7, 146.1, 144.3, 142.0, 140.4, 139.3, 137.9, 136.6, 135.6, 134.9, 128.2, 127.1, 126.2, 125.5, 125.2, 125.0, 124.4, 124.0, 123.9, (123.5, 123.4, 123.2), 122.7, 114.6, 114.2, 54.2, 53.8, (44.3, 44.2, 44.1, 43.9), (35.18, 35.13, 35.06, 35.02), (34.4, 34.3, 34.2), 34.0, 31.8, 30.5, (29.0, 28.9, 28.8, 28.7), (28.44, 28.40), (27.5, 27.4, 27.3), 27.1, (23.1, 23.0, 22.9), 22.8, 14.4, (14.32, 14.28), (10.99, 10.95), (10.85, 10.79), (10.64, 10.62, 10.58, 10.55, 10.52, 10.47). HR-ESI-MS (*m/z*): calcd for $C_{68}H_{92}N_2S_5$: 1096.5859. Found: 1096.5827 (M^+), 1110.6017 ($[M+Na]^+$).

5: To a solution of **4** (0.33 g, 0.30 mmol) in anhydrous THF (50 mL) was added a solution of lithium diisopropylamide in THF (10 mL, 0.60 mmol) dropwise in N_2 atmosphere at -78 ℃. The mixture was stirred at -78 ℃ for 1 h and Me_3SnCl (0.18 g, 0.90 mmol) in anhydrous THF (10 mL) was added. The mixture solution was warmed up to room temperature and stirred for 10 h. The mixture solution was quenched with water, and extracted with chloroform. The organic extracts were washed with brine

and dried over anhydrous Na_2SO_4. After removal of the solvent under the reduced pressure, the product was obtained as purple oil (0.34 g, 91%). ^{1}H NMR ($CDCl_3$, 400 MHz, ppm): δ 8.08-8.13 (m, 1H, Th-H), 8.02-8.04 (m, 1H, Th-H), 7.83-7.89 (d, d, *J* = 8.0 Hz, 2H, Ph-H), 7.38 (s, 1H, Ph-H), 7.33 (s, 1H, Ph-H), 7.19-7.20 (d, *J* = 3.6 Hz, 1H, Th-H), 7.11-7.12 (d, *J* = 3.6 Hz, 1H, Th-H), 7.03 (s, 1H, Th-H), 6.72-6.73 (d, *J* = 3.6 Hz, 1H, Th-H), 2.81-2.84 (t, *J* = 7.6 Hz, 2H, CH_2), 1.96-2.04 (m, 8H, CH_2), 1.69-1.73 (m, 2H, CH_2), 1.26-1.41 (m, 6H, CH_2), 0.54-0.95 (m, 63H, CH_2, CH_3), 0.39 (s, 9H, $Sn(CH_3)_3$). ^{13}C NMR ($CDCl_3$, 100 MHz, ppm): δ (157.4, 157.3), 155.8, (153.7, 153.6), 153.2, 152.9, 152.7, (148.02, 147.97), 146.1, (144.5, 144.4), (140.33, 140.29), 139.4, 139.3, 138.0, 136.6, 135.5, 135.0, 130.6, 128.2, 127.2, 125.5, 125.2, 125.0, 124.4, 124.0, 123.9, (123.6, 123.4, 123.3), 114.8, 114.4, 54.2, (53.21, 53.18), (44.3, 43.9), (35.3, 35.21, 35.18, 35.16, 35.1), (34.4, 34.3, 34.1), (31.80, 31.78), 30.5, 29.0, (28.94, 28.94, 28.89, 28.81, 28.76), (28.6, 28.5, 28.4), (27.7, 27.6), (27.52, 27.49, 27.42), 27.3, (23.1, 23.0), 22.8, (14.40, 14.35, 14.3, 14.29, 14.25), (10.94, 10.91), 10.8, (10.70, 10.68, 10.64, 10.62, 10.60, 10.57), (-8.01, -8.04, -8.08). HR-ESI-MS (*m/z*): calcd for $C_{71}H_{100}N_2S_5Sn$: 1260.5517 (M^+). Found: 1260.5516 (M^+).

7: In a 100 mL two-neck round-bottom flask, **2** (300 mg, ca. 0.30 mmol), **6** (150 mg, 0.30 mmol), and $Pd_2(dba)_3$ (13.5 mg, 0.015 mmol), tri(*o*-tolyl)phosphine (19.8 mg, 0.060 mmol) was added. The flask was evacuated and back-filled with N_2 three times, and then degassed toluene was injected into the mixture. The resulting solution was stirred at refluxing temperature for 12 h under the N_2 atmosphere. After being cooled to room temperature, the solvent was then removed under reduced pressure. The dark residue was purified by silica gel chromatography, eluting with PE-CH_2Cl_2 (20:1) to give purple oil (175 mg, 52%). ^{1}H NMR ($CDCl_3$, 400 MHz, ppm): δ 8.19-8.27 (m, 2H, Th-H), 7.44 (s, 1H, Ph-H), 7.36 (s, 1H, Ph-H), 7.24-7.26 (d, d, *J* = 4.8 Hz, 2H, Th-H), 7.15-7.16 (d, *J* = 3.6 Hz, 1H, Th-H), 6.99-7.00 (m, 1H, Th-H), 6.74-6.75 (d, *J* = 3.6 Hz, 1H, Th-H), 2.81-2.85 (t, *J* = 7.6 Hz, 2H, CH_2), 1.98-2.08 (m, 8H, CH_2), 1.68-1.75 (m, 2H, CH_2), 1.26-1.43 (m, 6H, CH_2), 0.87-0.95 (m, 36H, CH_2), 0.52-0.77 (m, 27H, CH_2, CH_3). ^{13}C NMR ($CDCl_3$, 100 MHz, ppm): δ (155.5, 155.4, 155.3), 155.2, (153.7, 153.6), 153.5, (151.4, 151.2, 148.9, 148.7, J_{CF} = 257, 20 Hz), (150.8, 150.7, 148.3, 148.1, J_{CF} = 257, 20 Hz), 149.1, 149.0, 146.9, 146.5, 142.0, (141.32, 141.25, J_{CF} = 7 Hz), 137.1, 135.4, 134.5, 132.7, (131.7, 131.6, J_{CF} = 10 Hz), 130.3, 126.6, 126.5, 125.2, 124.2, 123.4, 122.7, 114.9, 114.3, (112.9, 112.8, J_{CF} = 11 Hz), (110.8, 110.7, J_{CF} = 12 Hz), 54.2, 53.8, (44.3, 43.9), (35.24, 35.17, 35.09, 35.06), (34.5, 34.4, 34.3, 34.1), (31.81, 31.77), 30.5, (29.0, 28.9, 28.8), (28.5, 27.4), (27.7, 27.5, 27.4, 27.3, 27.2), (23.07, 23.05, 23.0, 22.95, 22.8), (14.4, 14.3, 14.2), (10.98, 10.94), (10.83, 10.79), (10.6, 10.54, 10.49). HR-ESI-MS (*m/z*): calcd for $C_{68}H_{90}N_2S_5F_2$: 1132.5670. Found: 1132.5687 (M^+).

8: To a solution of **7** (0.28 g, 0.25 mmol) in anhydrous THF (50 mL) was added a solution of lithium diisopropylamide in THF (10 mL, 0.50 mmol) dropwise in N_2 atmosphere at -78 ℃. The mixture was stirred at -78 ℃ for 1 h and Me_3SnCl (0.15 g, 0.75 mmol) in anhydrous THF (10 mL) was added. The mixture solution was warmed up to room temperature and stirred for 10 h. The mixture solution was quenched with water, and extracted with chloroform. The organic extracts were washed with brine and dried over anhydrous Na_2SO_4. After removal of the solvent under the reduced pressure, the product was obtained as purple oil (0.28 g, 89%). ^{1}H NMR ($CDCl_3$, 400 MHz, ppm): δ 8.20-8.26 (m, 2H, Th-H), 7.43 (s, 1H, Ph-H), 7.35 (s, 1H, Ph-H), 7.24-7.25 (d, *J* =3.6 Hz, 2H, Th-H), 7.15-7.16 (d, *J* = 3.6 Hz, 1H, Th-H), 7.03 (m, 1H, Th-H), 6.74-6.75 (d, *J* = 3.6 Hz, 1H, Th-H), 2.81-2.85 (t, *J* = 7.6 Hz, 2H, CH_2), 1.97-2.04 (m, 8H, CH_2), 1.70-1.74 (m, 2H, CH_2), 1.26-1.45 (m, 6H, CH_2), 0.56-0.75 (m, 63H, CH_2, CH_3), 0.40 (s, 9H, $Sn(CH_3)_3$). ^{13}C NMR ($CDCl_3$, 100 MHz, ppm): δ (157.6, 157.5), (155.2, 155.1), 153.8, 153.7, 153.5, (151.4, 151.2, 148.8, 148.7, J_{CF} = 258, 20 Hz), (150.8, 150.6, 148.0, 147.9, J_{CF} = 258, 18 Hz), 149.0, 148.9, (147.1, 147.0), 146.5, (141.3, 141.2, J_{CF} = 6 Hz), 139.7, 137.1, 135.2, 134.5, 132.5, (131.7, 131.6, J_{CF} = 9 Hz), 130.6, 130.3, (126.6, 126.5), 125.2, 124.2, 123.4, 115.1, 114.4, (112.9, 112.8, J_{CF} = 12 Hz), (110.7, 110.5, J_{CF} = 12 Hz), 54.2, 53.2, (44.3, 43.9), 35.1, (34.4, 34.2, 34.1), 31.8, 30.5, 29.9, (29.0, 28.9, 28.8, 28.7), (28.6, 28.4), (27,6, 27.5, 27.4, 27.3), (23.1, 23.0), 22.8, (14.4, 14.2), (10.9, 10.8, 10.7, 10.6). -8.07. HR-ESI-MS (*m/z*): calcd for $C_{71}H_{98}F_2N_2S_5Sn$: 1296.5324. Found: 1133.5774 ([M-$SnMe_3$]$^+$).

DPPBIT: In a 100 mL two-neck round-bottom flask, **5** (151 mg, 0.12 mmol), **9** (31.5 mg, 0.050 mmol), and $Pd_2(dba)_3$ (2.3 mg, 0.0025 mmol), tri(*o*-tolyl)phosphine (3.1 mg, 0.010 mmol) was added. The flask was evacuated and back-filled with N_2 three times, and then degassed toluene was injected into the mixture. The resulting solution was stirred at refluxing temperature for 12 h under the N_2 atmosphere. After being cooled to room temperature, the solvents were then removed under reduced pressure. The dark residue was purified by silica gel chromatography, eluting with PE-CH_2Cl_2 (3:1) to give dark solid (102 mg, 76%). ^{1}H NMR ($CDCl_3$, 400 MHz, ppm): δ 8.95-9.01 (m, 2H, Th-H), 8.09-8.15 (m, 2H, Th-H), 8.04 (m, 2H, Th-H), 7.85-7.91 (d, d, *J* = 7.6 Hz, 2H, Ph-H), 7.41 (s, 2H, Ph-H), 7.36 (m, 4H, Ph-H, Th-H), 7.26 (s, 2H, Th-H), 7.20-7.21 (d, *J* = 3.6 Hz, 2H, Th-H), 7.11-7.12 (d, *J* = 3.6 Hz, 2H, Th-H), 6.73-6.74 (d, *J* = 3.6 Hz, 2H, Th-H), 4.15 (m, 4H, *N*-CH_2), 2.81-2.85 (t, *J* = 7.6 Hz, 4H, CH_2), 2.01-2.06 (m, 16H, CH_2, CH), 1.83 (m, 4H, CH_2), 1.69-1.73 (m, 4H, CH_2), 1.51 (m, 4H, CH_2), 1.33-1.39 (m, 20H, CH_2), 0.91-0.96 (m, 76H, CH_2), 0.54-0.73 (m, 56H, CH_2, CH_3). ^{13}C NMR ($CDCl_3$, 125 MHz, ppm): δ 161.6, 156.5, 153.8, 153.5, 152.9, 152.8, 146.3, 144.4, 144.0, 143.7, 141.3, 139.5, 139.0, 137.9, 137.3, 137.0, 136.9, 136.8, 135.8, 135.0, 128.4, 127.8, 127.1, 125.5, 125.4, 125.2, 124.7, 124.3, 124.1, 124.0, 123.6, (123.4, 123.3), 120.8, 114.6, 108.5, 54.4, (44.4, 44.0), 42.6, 35.4, (34.6, 34.5), (34.4, 34.2, 34.1), (31.8, 31.7), 30.5, 30.2, (29.0, 28.9), 28.5, (27.64, 27.55, 27.4), 26.8, (23.10, 23.06), 22.8, (14.4, 14.3), (11.0, 10.9, 10.84, 10.79), 10.6. MALDI-TOF MS (*m/z*): calcd for $C_{162}H_{212}N_6O_2S_{12}$: 2658.3 ($M^+$, 100%). Found: 2659.4 ([M+H]$^+$, 100%). Elemental Analysis: calcd for $C_{162}H_{212}N_6O_2S_{12}$: C, 73.14; H, 8.03; N, 3.16. Found: C, 73.60; H, 8.10; N, 3.11.

DPPBIT4F: In a 100 mL two-neck round-bottom flask, **8** (156 mg, 0.12 mmol), **9** (31.4 mg, 0.050 mmol), and $Pd_2(dba)_3$ (4.6 mg, 0.005 mmol), tri(*o*-tolyl)phosphine (6.2 mg, 0.020 mmol) was added. The flask was evacuated and back-filled with N_2 three times, and then degassed toluene was injected into the mixture. The resulting solution was stirred at refluxing temperature for 12 h under the N_2 atmosphere. After being cooled to room temperature, the solvent were then removed under reduced

pressure. The dark residue was purified by silica gel chromatography, eluting with PE-CH_2Cl_2 (3:1) to give dark solid (110 mg, 81%). ^{1}H NMR ($CDCl_3$, 400 MHz, ppm): δ 8.95-9.01 (m, 2H, Th-H), 8.21-8.28 (m, 4H, Th-H), 7.46 (s, 2H, Ph-H), 7.36-7.37 (m, 4H, Ph-H, Th-H), 7.24-7.26 (m, 4H, Th-H), 7.16-7.17 (d, *J* = 3.6 Hz, 2H, Th-H), 6.74-6.75 (d, *J* = 3.6 Hz, 2H, Th-H), 4.15 (m, 4H, *N*-CH_2), 2.81-2.85 (t, *J* = 7.6 Hz, 4H, CH_2), 2.01-2.07 (m, 16H, CH_2, CH), 1.81-1.83 (m, 4H, CH_2), 1.68-1.73 (m, 4H, CH_2), 1.49-1.52 (m, 4H, CH_2), 1.31-1.41 (m, 20H, CH_2), 0.89-0.96 (m, 76H, CH_2), 0.55-0.75 (m, 56H, CH_2, CH_3). ^{13}C NMR ($CDCl_3$, 125 MHz, ppm): δ 162.0, 156.44, 156.37, 153.7, 153.4, 152.9, 152.8, 146.2, 144.3, 144.0, 143.6, 141.2, 139.4, 137.9, 137.3, 137.1, 136.7, 135.8, 134.9, 128.3, 127.7, 127.0, 125.5, 125.3, 125.2, 124.7, 124.11, 124.07, 124.0, 123.5, 123.4, 123.2, 120.7, 114.6, 114.5, 108.6, 54.4, 54.3, 46.3, 44.3, 43.9, 39.6, (35.4, 35.31, 35.26), (34.5, 34.4), (34.3, 34.2), (31.8, 31.7), 30.7, 30.5, (29.0, 28.9, 28.8), 28.4, (27.6, 27.5, 27.4, 27.3), 24.0, 23.4, (23.1, 23.03, 23.00), 22.8, (14.39, 14.35, 14.29, 14.25), (11.0, 10.9, 10.84, 10.77, 10.6). MALDI-TOF MS (m/z): calcd for $C_{162}H_{208}F_4N_6O_2S_{12}$: 2729.3. Found: 2729.9 (M^+). Elemental Analysis: calcd for $C_{162}H_{208}F_4N_6O_2S_{12}$: C, 71.21; H, 7.67; N, 3.08. Found: C, 71.09; H, 7.64; N, 2.94.

Acknowledgements

This work was financially supported by the grants from the National Natural Science Foundation of China (21202007, 21472012, 51225301, 91333206); the Thousand Youth Talents Plan of China; Beijing Natural Science Foundation (2152027), the Development Program for Distinguished Young and Middle-aged Teachers and Special programs to cultivate major projects of Beijing Institute of Technology.

Notes and references

[a]*Beijing Key Laboratory of Photoelectronic/Electrophotonic Conversion Materials, Key Laboratory of Cluster Science of Ministry of Education, School of Chemistry, Beijing Institute of Technology, 5 South Zhongguancun Street, Beijing, 100081, China.*
E-mail: jinlwang@bit.edu.cn
[b]*Institute of Polymer Optoelectronic Materials and Devices, State Key Laboratory of Luminescent Materials and Devices, South China University of Technology, 381 Wushan Road, Guangzhou, 510640, China.*
E-mail: hbwu@scut.edu.cn
[+] These authors contributed equally to this work.

† Electronic Supplementary Information (ESI) available: See DOI: 10.1039/b000000x/

1 a) O. Inganäs, F. Zhang and M. R. Andersson, *Acc. Chem. Res.*, 2009, **42**, 1731; b) H.-Y. Chen, J. Hou, S. Zhang, Y. Liang, G. Yang, Y. Yang, L. Yu, Y. Wu and G. Li, *Nat. Photon.*, 2009, **3**, 649; c) P. M. Beaujuge and J. M. J. Fréchet, *J. Am. Chem. Soc.*, 2011, **133**, 20009; d) Y. Li, *Acc. Chem. Res.*, 2012, **45**, 723; e) H. Zhou, L. Yang, W. You, *Macromolecules*, 2012, **45**, 607; f) Z. He, C. Zhong, S. Su, M. Xu, H. Wu and Y. Cao, *Nat. Photon.*, 2012, **6**, 593; g)Y. Li, *Acc. Chem. Res.*, 2012, **45**, 723; h) C. Cabanetos, A. E. Labban, J. A. Bartelt, J. D. Douglas, W. R. Mateker, J. M. J. Fréchet, M. D. McGehee and P. M. Beaujuge, *J. Am. Chem. Soc.*, 2013, **135**, 4656; i) K. Li, Z. Li, K. Feng, X. Xu, L.Wang, and Q. Peng, *J. Am. Chem. Soc.* 2013, **135**, 13549; j) I. Osaka, T. Kakara, N. Takemura, T. Koganezawa and K. Takimiya, *J. Am. Chem. Soc.*, 2013, **135**, 8834; k) K. H. Hendriks, G. H. L. Heintges, V. S. Gevaerts, M. M. Wienk and R. A. J. Janssen, *Angew. Chem. Int. Ed.*, 2013, **52**, 8341; l) L. Ye, S. Zhang, L. Huo, M. Zhang and J. Hou, *Acc. Chem. Res.*, 2014, **47**, 1595; m) T. Qin, W. Zajaczkowski, W. Pisula, M. Baumgarten, M. Chen, M. Gao, G. Wilson, C. D. Easton, K. Müllen and S. E. Watkins, *J. Am. Chem. Soc.*, 2014, **136**, 6049; n) K. Mazzio and C. K. Luscombe, *Chem. Soc. Rev.* 2015, **44**, 78.

2 a) J.-D. Chen, C. Cui, Y.-Q. Li, L. Zhou, Q.-D. Ou, C. Li, Y. Li and J. –X. Tang, *Adv. Mater.*, 2014, DOI: 10.1002/adma.201404535; b) Y. Liu, J. Zhao, Z. Li, C. Mu, W. Ma, H. Hu, K. Jiang, H. Lin, H. Ade and H. Yan, *Nature Commun*. 2014, DOI: 10.1038/ncomms6293; c) L. Ye, S. Zhang, W. Zhao, H. Yao and J. Hou, *Chem. Mater.*, 2014, **26**, 3603; d) T. L. Nguyen, H. Choi, S.-J. Ko, M. A. Uddin, B. Walker, S. Yum, J.-E. Jeong, M. H. Yun, T. J. Shin, S. Hwang, J. Y. Kim and H. Y. Woo, *Energy Environ. Sci.* 2014, **7**, 3040.

3 For reviews, see a) C. Li, M. Liu, N. G. Pschirer, M. Baumgarten and K. Müllen, *Chem. Rev.* 2010, **110**, 6817; b) B. Walker, C. Kim and T.-Q. Nguyen, *Chem. Mater.* 2011, **23**, 470; c) A. Mishra and P. Bäuerle, *Angew. Chem. Int. Ed.*, 2012, **51**, 2020; d) Y. Lin, Y. Li and X. Zhan, *Chem. Soc. Rev.*, 2012, **41**, 4245; e) Y. Chen, X. Wan and G. Long, *Acc. Chem. Res.*, 2013, **46**, 2645; f) J. E. Coughlin, Z. B. Henson, G. C. Welch and G. C. Bazan, *Acc. Chem. Res.*, 2014, **47**, 257; g) J. Roncali, P. Leriche and P. Blanchard, *Adv. Mater.*, 2014, **26**, 3821; h) A. F. Eftaiha, J.-P. Sun, I. G. Hill and G. C.Welch, *J. Mater. Chem. A.*2014, **2**, 1201.

4 a) L. Bu, X. Guo, B. Yu, Y. Qu, Z. Xie, D. Yan, Y. Geng, F. Wang, *J. Am. Chem. Soc.*, 2009, **131**, 13242; b) F. G. Brunetti, X. Gong, M. Tong, A. J. Heeger and F. Wudl, *Angew. Chem. Int. Ed.*, 2010, **49**, 532. c) H. Shang, H. Fan, Y. Liu, W. Hu, Y. Li and X. Zhan, *Adv. Mater.*, 2011, **23**, 1554; d) M. Seri, A. Marrocchi, D. Bagnis, R. Ponce, A. Taticchi, T. J. Marks and A. Facchetti, *Adv. Mater.*, 2011**. 23**, 3827; e) T. Bura, N. Leclerc, S. Fall, R. Lévêque, T. Heiser, P. Retailleau, S. Rihn, A. Mirloup, R. Ziessel, *J. Am. Chem. Soc.*, 2012, **134**, 17404; f) H. Bürckstummer, E. V. Tulyakova, M. Deppisch, M. R. Lenze, N. M. Kronenberg, M. Gsänger, M. Stolte, K. Meerholz, F. Würthner, *Angew. Chem. Int. Ed.*, 2011, **50**, 11628; g) X. Xiao, G. Wei, S. Wang, J. D. Zimmerman, C. K. Renshaw, M. E. Thompson, S. R. Forrest, *Adv. Mater.*, 2012, **24**, 1956; h) S. Shen, P. Jiang, C. He, J. Zhang, P. Shen, Y. Zhang, Y. Yi, Z. Zhang, Z. Li, Y. Li, *Chem. Mater.*, 2013, **25**, 2274; i) X. Liu, Q. Li, Y. Li, X. Gong, S.-J. Su and Y. Cao, *J. Mater. Chem. A.*, 2014, **2**, 4004; j) H. Bai, Y. Wang, P. Cheng, Y. Li, D. Zhu and X. Zhan, *ACS Appl. Mater. Interfaces* 2014, **6**, 8426; k) Y. R. Cheon, Y. J. Kim, J. Y. Back, T. K. An, C. E. Park and Y.-H. Kim, *J. Mater. Chem. A.*, 2014, **2**, 16443; l) L. Liang, J.-T. Wang, X. Xiang, J. Ling, F.-G. Zhao and W.-S. Li, *J. Mater. Chem. A.*, 2014, **2**, 15396; m) D. Liu, M. Xiao, Z. Du, Y. Yan, L. Han, V. A. L. Roy, M. Sun, W. Zhu, C. S. Lee and R. Yang, *J. Mater. Chem. A.*, 2014, **2**, 7523; n) K. Lim, S. Y. Lee, K. Song, G. D. Sharma and J. Ko, *J. Mater. Chem. C.*, 2014, **2**, 8412; o) N. Lim, N. Cho, S. Paek, C. Kim, J. K. Lee and J. Ko, *Chem. Mater.*, 2014, **26**, 2283; p) L. Chen, L. Huang, D. Yang, S. Ma, X. Zhou, J. Zhang, G. Tu and C. Li, *J. Mater. Chem. A.*, 2014, **2**, 2657.

5 a) Y. Sun, G. C. Welch, W. L. Leong, C. J. Takacs, G. C. Bazan and A. J. Heeger, *Nat. Mater.* 2012**, 11**, 44; b) T. S. van der Poll, J. A. Love, T.-Q. Nguyen and G. C. Bazan, *Adv. Mater***. 2012, 24**, 3646; c) A. K. K. Kyaw, D. H. Wang, D. Wynands, J. Zhang, T.-Q. Nguyen, G. C. Bazan and A. J. Heeger, *Nano Lett.* 2013**, 13**, 3796; d) X. Liu, Y. Sun, B. B.Y. Hsu, A. Lorbach, L. Qi,; A. J. Heeger and G. C. Bazan, *J. Am. Chem. Soc.* 2014, **136**, 5697; e) J. A. Love, I. Nagao, Y. Huang, M. Kuik, V. Gupta, C. J. Takacs, J. E. Coughlin, L. Qi, T. S.van der Poll, E. J. Kramer, A. J. Heeger, T.-Q. Nguyen and G. C. Bazan, *J. Am. Chem. Soc.* 2014, **136**, 3597; f) Y. Liu, X. Wan, F. Wang, J. Zhou, G. Long, J. Tian and Y. Chen, *Adv. Mater.* 2011**, 23**, 5387; g) J. Zhou, X. Wan, Y. Liu, Y. Zuo, Z. Li, G. He, G. Long, W. Ni, C. Li, X. Su and Y. Chen, *J. Am. Chem. Soc.* 2012**, 134**, 16345; h) J. Zhou, Y. Zuo, X. Wan, G. Long, Q. Zhang, W. Ni, Y. Liu, Z. Li, G. He, C. Li, B. Kan, M. Li and Y. Chen, *J. Am. Chem. Soc.* 2013, **135**, 8484; i) Y. Liu, C.-C. Chen, Z. Hong, J. Gao, Y. Yang, H. Zhou, L. Dou, G. Li and Y. Yang, *Sci. Rep.* 2013**, 3**, 3356; j) B. Kan, Q. Zhang, M. Li, X. Wan, W. Ni, G. Long, Y. Wang, X. Yang, H. Feng and Y. Chen, *J. Am. Chem. Soc.* 2014**, 136**,15529; k) Q. Zhang, B. Kan, F. Liu, G. Long, X. Wan, X. Chen, Y. Zuo, W. Ni, H. Zhang, M. Li, Z. Hu, F. Huang, Y. Cao, Z. Liang, M. Zhang, T. P. Russell and Y. Chen, *Nature Photon.* 2014, DOI: 10.1038/NPHOTON. 2014.269; l) H. Qin, L. Li, F. Guo, S. Su, J. Peng, Y. Cao and X. Peng, *Energy Environ. Sci.* 2014, **7**, 1397; m) Z. Du, W. Chen, Y. Chen, S. Qiao, X. Bao, S. Wen, M. Sun, L. Han and R. Yang,

J. Mater. Chem. A., 2014, **2**, 15904; n) X. Xu, A. K. K. Kyaw, B. Peng, Q. Du, L. Hong, H. V. Demir, T. K. S. Wong, Q. Xiong and X. W. Sun, *Chem. Commun.* 2014, **50**, 4451.

6 a) B.Walker, A. B. Tamayo, X.-D. Dang, P. Zalar, J. H. Seo, A. Garcia, M. Tantiwiwat and T.-Q. Nguyen, *Adv. Funct. Mater.*, 2009, **19**, 3063; b) S. Qu and H. Tian, *Chem. Commun.*, 2012, **48**, 3039; c) J. Liu, Y. Sun, P. Moonsin, M. Kuik, C. M. Proctor, J. Lin, B. B. Hsu, V. Promarak, A. J. Heeger and T.-Q. Nguyen, *Adv. Mater.*, 2013, **25**, 5898; d) Y. Li, P. Sonar, L. Murphy and W. Hong, *Energy Environ. Sci.* 2013, **6**, 1684; e) J. Huang, C. Zhan, X. Zhang, Y. Zhao, Z. Lu, H. Jia, B. Jiang, J. Ye, S. Zhang, A. Y. Tang, Liu, Q. Pei and J. Yao, *ACS Appl. Mater. Interfaces*, 2013, **5**, 2033; f) Y. Lin, Y. Li and X. Zhan, *Adv. Energy. Mater.*, 2013, **3**, 724; g) V. S. Gevaerts, E. M. Herzig, M. Kirkus, K. H. Hendriks, M. M. Wienk, J. Perlich, P. Müller-Buschbaum and R. A. J. Janssen, *Chem. Mater.* 2014, **26**, 916; h) Q.-C. Yu, W.-F. Fu, J.-H. Wan, X.-F. Wu, M.-M. Shi and H.-Z. Chen, *ACS Appl. Mater. Interfaces*, 2014, **6**, 5798; i) L. Fu, W. Fu, P. Cheng, Z. Xie, C. Fan, M. Shi, J. Ling, J. Hou, X. Zhan and H. Chen, *J. Mater. Chem. A.*, 2014, **2**, 6589; j) Y. S. Park, T. S. Kale, C.-Y. Nam, D. Choi and R. B. Grubbs, *Chem. Commun.*, 2014, **50**, 7964; k) H. Gao, Y. Li, L. Wang, C. Ji, Y. Wang, W. Tian, X. Yang and L. Yin, *Chem. Commun.*, 2014, **50**, 10251; l) Y. Yang, G. Zhang, C. Yu, C. Yu, C. He, J. Wang, X. Chen, J. Yao, Z. Liu and D. Zhang, *Chem. Commun.*, 2014, **50**, 9939; m) W. Shin, T. yasuda, Y. hidaka, G. Watanabe, R. Arai, K. Nasu, T. Yamaguchi, W. Murakami, K. Makita and C. Adachi, *Adv. Energy. Mater.*, 2014, 1400879; n) D. Yoo, B. Nketia-Yawson, S.-J. Kang, H. Ahn, T. J. Shin, Y.-Y. Noh and C. Yang, *Adv. Funct. Mater.* 2015, **25**, 586; o) W. Li; K. H. Hendriks, A. Furlan, M. M. Wienk and R. A. J. Janssen, *J. Am. Chem. Soc.*, 2015, **137**, 2231; p) K. A. Mazzio, M. Yuan, K. Okamoto and C. K. Luscombe, ACS Appl. Mater. Interfaces 2011, **3**, 271.

7 a) S. Albrecht, S. Janietz, W. Schindler, J. Frisch, J. Kurpiers, J. Kniepert, S. Inal, P. Pingel, K. Fostiropoulos, N. Koch and D. Neher, *J. Am. Chem. Soc.*, 2012, **134**, 14932; b) J. R. Tumbleston, H. Zhou, W. Li, S. Liu, H. Ade and W. You, *J. Am. Chem. Soc.*, 2013, **135**, 1806; c) J. H. Park, E. H. Jung, J. W. Jung and W. H. Jo, *Adv. Mater.*, 2013, **25**, 2583; d) N.Wang, Z. Chen, W. Wei and Z. Jiang, *J. Am. Chem. Soc.* 2013, **135**, 17060; e) P. Liu, K. Zhang, F. Liu, Y. Jin, S. Liu, S. Liu, T. P. Russell, H.-L. Yip, F. Huang and Y. Cao, *Chem. Mater.*, 2014, **26**, 2009; f) M. Zhang, X. Guo, S. Zhang, J. Hou, *Adv. Mater.*, 2014, **26**, 1118; g) Y. Deng, J. Liu, J. Wang, L. Liu, W. Li, H. Tian, X. Zhang, Z. Xie, Y. Geng and F. Wang, *Adv. Mater.* 2014, **26**, 471.

8 a) J. J. Intemann, K. Yao, H.-L.Yip, Y.-X. Xu, Y.-X. Li, P.-W. Liang, F.-Z. Ding, X. Li, A. K.-Y. Jen, *Chem. Mater.*, 2013, 25, 3188; b) Y.-H. Chao, J.-F. Jheng, J.-S.Wu, K.-Y. Wu, H.-H. Peng, M.-C. Tsai, C.-L. Wang, Y.-N. Hsiao, C.-L. Wang, C.-Y. Lin and C.-S. Hsu, *Adv. Mater.*, 2014, 26, 5205; c) H. Zhou, L. Yang, A. C. Stuart. S. C. Price, S. Liu and W. You, *Angew. Chem. Int. Ed.* 2011, 50, 2995; d) K. Li, Z. Li, K. Feng, X. Xu, L. Wang and Q. Peng, *J. Am. Chem. Soc.* 2013, 135, 13549; e) J. Lee, M. Jang, S. M. Lee, D. Yoo, T. J. Shin, J. H. Oh and C. Yang, *ACS Appl. Mater. Interfaces* 2014, 6, 20390; f) R. S. Ashraf, B. C. Schroeder, H. A. Bronstein, Z. Huang, S. Thomas, R. J. Kline, C. J. Brabec, P. Rannou, T. D. Anthopoulos, J. R. Durrant and I. McCulloch, *Adv. Mater.* 2013, 25, 2029; g) B. Carsten, J. M. Szarko, H. J. Son, W. Wang, L. Lu, F. He, B. S. Rolczynski, S. J. Lou, L. X. Chen, L. Yu, *J. Am. Chem. Soc.* 2011, 133, 20468; h) P. Yang, M. Yuan, D. F. Zeigler, S. E. Watkins, J. A. Lee and C. K. Luscombe, *J. Mater. Chem. C.* 2014, 2, 3278.

9 H. Bronstein, D. S. Leem, R. Hamilton, P. Woebkenberg, S. King, W. Zhang, R. S. Ashraf, M. Heeney, T. D. Anthopoulos, J. de. Mello and I. McCulloch, *Macromolecules*, 2011, **44**, 6649.

10 a) M. Melucci, L. Favaretto, A. Zanelli, M. Cavallini, A. Bongini, P. Maccagnani, P. Ostoja, G. Derue, R. Lazzaroni and G. Barbarella, *Adv. Funct. Mater.* 2010, **20**, 445; b) J.-L.Wang, Q.-R.Yin, J.-S. Miao, Z. Wu, Z.-F. Chang, Y. Cao, R.-B. Zhang, J.-Y. Wang, H.-B. Wu and Y. Cao, *Adv. Funct. Mater.*10.1002/adfm.201500190.

11 H. Bronstein, J. M. Frost, A. Hadipour, Y. Kim, C. B. Nielsen, R. S. Ashraf, B. P. Rand, S. Watkins, I. McCulloch, *Chem. Mater*,. 2013, **25**, 277.

12 a) J. Liu, L. Chen, B. Gao, X. Cao, Y. Han, Z. Xie and L.Wang, *J. Mater. Chem. A*, **2013**, *1*, 6216; b) C. D. Wessendorf, G. L. Schulz, A. Mishra, P. Kar, I. Ata, M. Weidelener, M. Urdanpilleta, J. Hanisch, E. Mena-Osterita, M. Lindén, E. Ahlswede and P. Bäuerle, *Adv. Energy Mater.*, 2014, **4**, 1400266; c) K. Sun; Z. Xiao, E. hanssen, M. F. G. Klein, H. H. Dam, M. Pfaff, D. Gerthsen, W. W. H. Wong and D. J. Jones, *J. Mater. Chem. A*, 2014, **2**, 9048; d) T. A. Bull, L. S. C. Pingree, S. A. Jenekhe, D. S. Ginger and C. K. Luscombe, ACS Nano. 2009, **3**, 627.

13 a) J. D. Zimmerman, X. Xiao, C. K. Renshaw, S. Wang, V. V. Diev, M. E. Thompson and S. R. Forrest, *Nano. Lett.* 2012, **12**, 4366; b) M. M. Mandoc, L. J. A. Koster and P. W. M. Blom, *Appl. Phys. Lett.* 2007, **90**, 133504.

14 a) G. Wei, S. Wang, K. Sun, M. E. Thompson and S. R. Forrest, *Adv. Energy. Mater.*, 2011, **1**, 184; b) G. Li, V. Shrotriya, J. Huang, Y. Yao, T. Moriarty, K. Emery and Y. Yang, *Nat. Mater.* 2005, **4**, 864.

15 a) D. Patra, C.-C. Chiang, W.-A. Chen, K.-H. Wei, M.-C. Wu and C.-W. Chu, *J. Mater. Chem. A.*, 2013, **1**, 7767; b) C. M. Proctor, J. A. Love and T.-Q. Nguyen, *Adv. Mater.*, 2014, **26**, 5957.

16 A. K. K. Kyaw, D. H. Wang, C. Luo, Y. Cao and A. J. Heeger, *Adv. Energy Mater.*, 2014, **4**, 1301469.

17 Z. C. He, C. M. Zhong, X. Huang, W.-Y. Wong, H. B. Wu, L. W. Chen, S. J. Su and Y. Cao, *Adv. Mater.*, 2011, **23**, 4636.

Cite this: DOI: 10.1039/c0xx00000x

www.rsc.org/xxxxxx

ARTICLE TYPE

TOC:
The high PCE of **DPPBIT4F** with $PC_{71}BM$ on solvent vapor annealing proved that the introduction of multiple fluorine atoms on the weaker accepting units of extened molecules is still valid design strategy for high performance OSCs.

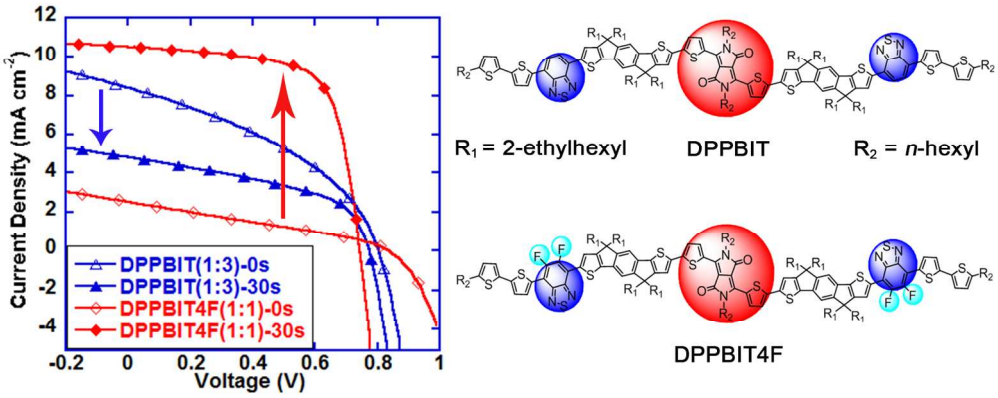

TOC